Exploring main group metal borosulfates: similarities and differences of two new borosulfates M[B2O(SO4)3] (M = Sr, Pb)

Philip Netzsch, Peter Gross, Hirotaka Takahashi, Sogol Lotfi, Jakoah Brgoch, Henning A. Höppe

Angaben zur Veröffentlichung / Publication details:

Netzsch, Philip, Peter Gross, Hirotaka Takahashi, Sogol Lotfi, Jakoah Brgoch, and Henning A. Höppe. 2019. “Exploring main group metal borosulfates: similarities and differences of two new borosulfates M[B2O(SO4)3] (M = Sr, Pb).” European Journal of Inorganic Chemistry 2019 (36): 3975–81. https://doi.org/10.1002/ejic.201900838.

ChemPubSoc Europe

DOI: 10.1002/ejic.201900838

EurJIC European Journal of Inorganic Chemistry

Full Paper

Borosulfates

Exploring Main Group Metal Borosulfates: Similarities and Differences of Two New Borosulfates $M[B_2O(SO_4)_3]$ (M = Sr, Pb)

Philip Netzsch,[a] Peter Gross,[a] Hirotaka Takahashi,[a] Sogol Lotfi,[b] Jakoah Brgoch,[b] and Henning A. Höppe*[a]

Abstract: The first strontium borosulfate $Sr[B_2O(SO_4)_3]$ and a novel lead borosulfate $Pb[B_2O(SO_4)_3]$ were obtained by solvothermal reaction of the respective anhydrous metal chlorides MCl_2 (M = Sr, Pb) with $H[B(HSO_4)_4]$ at 300 °C. The crystal structure of $Sr[B_2O(SO_4)_3]$ [*Pnma*, Z = 4, a = 1657.38(27) pm, b = 1203.68(19) pm, c = 439.484(8) pm] is isotypic with $Ba[B_2O(SO_4)_3]$ and consists of chains, built up by three membered rings of two borate tetrahedra and a sulfate tetrahedron. These rings are further connected via corner-sharing sulfate tetrahedra and hence can be classified as loop branched *zweier* double chains. $Pb[B_2O(SO_4)_3]$ crystallizes in a new structure type [$P2_1/m$, Z = 2, a = 440.00(2) pm, b = 1210.19(5) pm, c = 860.43(4) pm, β = 103.587(2) °] closely related to $Sr[B_2O(SO_4)_3]$. Both structures share the common supergroup *Pnmm* and basically differ by the orientation of adjacent anionic chains. The coordination surrounding of Pb^{2+} indicates a lone pair activity and DFT calculations confirmed a weak polarizability. Moreover, the compounds were characterized by electrostatic calculations, vibrational spectroscopy and thermal analysis and broaden the structural and chemical diversity of borosulfates.

Introduction

A relatively new representative of silicate-analogous materials are borosulfates, consisting of corner-sharing borate and sulfate tetrahedra.[1] Besides their vast structural diversity,[2] borosulfates feature weak ligand field splitting and weak nephelauxetic effects, confirmed by the absorption properties of transition metal borosulfates $M_4[B_2O(SO_4)_6]$ (M = Co, Ni)[3] and the luminescence properties of $RE_2[B_2(SO_4)_6]$ (RE = Ce, Eu, Tb).[4] In this rapidly growing compound class, only a few main group metals remain for which borosulfates are not known yet. Among these, strontium might be a quite interesting one as similar silicate-analogous materials have been identified as excellent host structures for phosphors.[5] Especially Sr^{2+} compounds like $SrSi_5N_8$:Eu^{2+},[6] $SrSi_2O_2N_2$:Eu^{2+}[7] and $Sr_6[B(PO_4)_4]$-$[PO_4]$:Eu^{2+}[8] are well suited hosts as they provide proper sites for the emissive Eu^{2+} ion comprising tunable luminescence, which is due to the same charge and their very similar ionic radii [$r_{ion}(Sr^{2+})$ = 136 pm, $r_{ion}(Eu^{2+})$ = 135 pm].[9]

Up to now, borosulfates of alkaline earth metals are known for magnesium, calcium and barium.[3,10,11] There are already two polymorphs for magnesium, viz. α-$Mg_4[B_2O(SO_4)_6]$ and β-$Mg_4[B_2O(SO_4)_6]$, comprising molecular $[B_2O(SO_4)_6]^{8-}$ units and a further magnesium borosulfate $Mg[B_2(SO_4)_4]$ containing a layered anion.[3] A very similar layered structure was described for calcium borosulfate $Ca[B_2(SO_4)_4]$.[10] Furthermore, barium borosulfate $Ba[B_2O(SO_4)_3]$ consists of infinite chains.[11] Strontium borosulfate was already postulated in 1962 by Schott and Kibbel, described as tris(sulfato)borate $Sr[B_2O(SO_4)_3]$.[12] However, the composition was only based on the mass percentage of the respective elements and only an assumption of a molecular borosulfate anion was given. Throughout their investigations, they also mentioned a lead borosulfate $Pb[B_2(SO_4)_4]$ with a different composition of the anion. Recently the respective crystal structure for this lead compound was elucidated and hence, the composition could be confirmed.[13]

Strontium and lead compounds often adopt similar structures; e.g. in the closely related compound class of borophosphates isotypic compounds were found for $M[BO(PO_4)]$ with M = Sr, Ba and Pb.[14] However, in nitridosilicates, the crystal structures of $Sr_2Si_5N_8$[15] and $Pb_2Si_5N_8$[16] are only isopointal, due to the formation of Pb_2 dumbbells. Furthermore, lone pair activity of s^2-ions might influence the surrounding framework like in recently reported $SnB_2O_3F_2$, where unique layers of condensed BO_3F-tetrahedra yield an excellent non-linear optical SHG effect.[17]

Herein we report the syntheses, crystal structures, selected spectroscopic properties, thermal behavior and results of DFT calculations on the electronic structures of the very first strontium borosulfate and a quite closely related new lead borosulfate.

[a] *Lehrstuhl für Festkörperchemie, Universität Augsburg, Universitätsstraße 1, 86159 Augsburg, Germany*
E-mail: henning.hoeppe@physik.uni-augsburg.de
https://www.ak-hoeppe.de
[b] *Department of Chemistry, University of Houston, Houston, TX 77204, USA*

Supporting information and ORCID(s) from the author(s) for this article are available on the WWW under https://doi.org/10.1002/ejic.201900838.

Results and Discussion

Crystal Structure

$Sr[B_2O(SO_4)_3]$ crystallizes in space group *Pnma* (No. 62) isotypically with $Ba[B_2O(SO_4)_3]$ (Figure 1, 2 and S1a).[11] The structure consists of loop branched *zweier* double chains comprising the fundamental building unit $[B_2O(SO_4)_3]^{2-}$. These chains are built up by three membered rings of two corner sharing borate tetrahedra and a sulfate tetrahedron and hence violate *Loewenstein*'s rule.[18] These rings are further connected via two sulfate tetrahedra forming chains with alternating direction along [001] (Figure 1). A similar basic building unit was also found in the mineral *stillwellite* $CeBO[SiO_4]$[19] and in the borophosphate $[Co(en)_3][B_2P_3O_{11}(OH)_2]$,[20] however, with a different connection pattern (Figure S3). Neglecting the loop branching of the present chain, this structure motif is reminiscent of the unbranched *zweier* double chains consisting of *sechser* rings, present in the mineral *tremolite* $Mg_5Ca_2[Si_4O_{11}]_2(OH)_2$ (Figure S2).[21] Nevertheless, an identical chain with respect to the borosulfate is unknown for silicates so far.

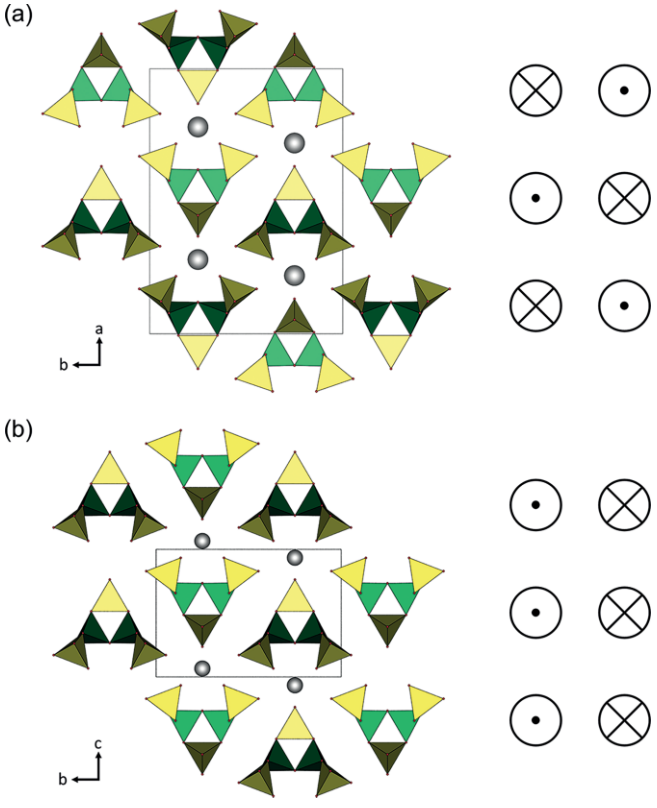

Figure 1. Crystal structure of $Sr[B_2O(SO_4)_3]$ viewed along $[00\bar{1}]$ (a) and of $Pb[B_2O(SO_4)_3]$ along [100] (b) with a schematic sketch of the orientation of the chains; borate tetrahedra green, sulfate tetrahedra yellow and metal cations gray.

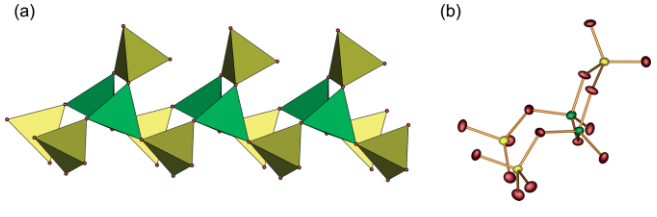

Figure 2. Part of the chains in $Sr[B_2O(SO_4)_3]$ and $Pb[B_2O(SO_4)_3]$ (color code as in Figure 1) (a) and fundamental building unit (b).

The deviation from the tetrahedral symmetry was calculated according to Balic Zunic and Makovicky.[22,23] This ranges for the sulfate tetrahedra from –0.08 to –0.12 % and amounts for the borate tetrahedron to –0.39 %; thus all tetrahedra can be classified as regular.

Chain like structures are known for borosulfates like $H_3O[B(SO_4)_2]$, where four membered rings of alternating borate and sulfate tetrahedra are present.[24] However, in $Sr[B_2O(SO_4)_3]$ the corner sharing borate tetrahedra lead to an even lower B/S ratio of 2:3, which is the smallest ratio so far for ionic borosulfates. The Sr^{2+} cations are situated between the chains. The coordination polyhedron of a tetra-capped trigonal prism is built up by nine oxygen terminal atoms stemming from sulfate tetrahedra and one bridging oxygen atom from a borate tetrahedron (Figure 3). This is, together with $Cs_2[B_2O(SO_4)_3]$ and $Rb_4[B_2O(SO_4)_4]$, one of the rare examples among the borosulfate family, where oxygen atoms stemming from borate tetrahedra are coordinating.[25] The Sr–O distances range between 251 and 281 pm and are in accordance with the sum of ionic radii (ΣIR = 271 pm) (Table 1).[9]

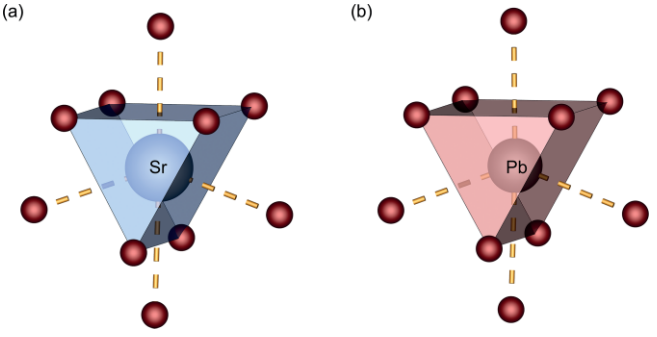

Figure 3. Tetracapped trigonal prismatic coordination environment for Sr (a) and Pb (b).

Table 1. Selected interatomic distances (in pm) and angles (in °) in the compounds $Sr[B_2O(SO_4)_3]$ and $Pb[B_2O(SO_4)_3]$ (esds in parentheses).

	$Sr[B_2O(SO_4)_3]$	$Pb[B_2O(SO_4)_3]$
M–O	251.39(25)-281.21(32)	250.49(19)-296.02(15)
$\Sigma r_{ion}(M–O)$[9]	271	275
S-O_{br}	151.42(29)-152.85(31)	151.72(13)-151.92(12)
S-O_{term}	142.57(29)-144.56(42)	142.36(19)-145.03(18)
B–O	141.21(47)-150.41(52)	140.8(2)-150.1(2)
O-S-O	103.28(17)-115.04(19)	102.94(7)-115.34(9)
O-B–O	103.09(31)-115.05(37)	102.84(12)-114.88(15)

$Pb[B_2O(SO_4)_3]$ crystallizes in a new structure type in space group $P2_1/m$ (No. 11) and is closely related to $Sr[B_2O(SO_4)_3]$ and $Ba[B_2O(SO_4)_3]$ (Figure S1b).[11] Accordingly, it is also built up by double chains of borate and sulfate tetrahedra. All tetrahedra can be classified as regular ones as the deviation from tetrahedral symmetry[22,23] for the sulfate tetrahedra ranges between –0.13 and –0.09 %, and for the borate tetrahedron amounts to

–0.30 %. Whereas in $Sr[B_2O(SO_4)_3]$ the direction of these chains is alternating, in $Pb[B_2O(SO_4)_3]$ the stacked chains proceed along the same direction leading to a smaller unit cell (Figure 1). The symmetry relation of both structures can be understood employing the common supergroup *Pnmm*. With respect to *Pnmm* the structure of $Sr[B_2O(SO_4)_3]$ adopts a *klassengleiche* subgroup with a doubling of the *c*-axis, whereas the space group of $Pb[B_2O(SO_4)_3]$ is a *translationengleiche* subgroup. The cations are situated on site symmetry *m* with a similar tetra-capped trigonal prismatic surrounding as the cations in $Sr[B_2O(SO_4)_3]$ (Figure 3). However, in $Pb[B_2O(SO_4)_3]$ two Pb–O distances (296 pm) of the upper chain are significantly longer than the sum of the ionic radii (ΣIR = 275 pm),[9] which are on the opposite side of the three shortest Pb–O distances (250–255 pm) (Figure S4). Hence, the structural changes indicate a slight lone-pair activity of Pb^{2+}.

Electrostatic Calculations

Both crystal structures were checked for electrostatic consistency by calculations based on the MAPLE concept (*MAPLE* = Madelung Part of Lattice Energy).[26] Therefore, the MAPLE values of the presented structures were calculated and compared to the sum of the MAPLE values of chemical similar binary and ternary compounds. A structure can be seen as electrostatically reasonable if the deviation of both values is below 1 %, which is the case for both compounds (Table 2). Furthermore, the calculations prove the coordination number of ten for both metal cations. The aforementioned two oxygen atoms with a longer Pb–O distance also show a significantly weaker contribution (Table S5).

Table 2. MAPLE calculations of the borosulfates $Sr[B_2O(SO_4)_3]$ and $Pb[B_2O(SO_4)_3]$ and their respective metal sulfates and boron oxide sulfate.

$Sr[B_2O(SO_4)_3]$ MAPLE = 115881 kJ mol^{-1} (Δ = 0.8 %)	$SrSO_4$[27] + $B_2S_2O_9$[28] MAPLE = 114938 kJ mol^{-1}
$Pb[B_2O(SO_4)_3]$ MAPLE = 115919 kJ mol^{-1} (Δ = 0.2 %)	$PbSO_4$[29] + $B_2S_2O_9$[28] MAPLE = 115742 kJ mol^{-1}

Infrared Spectroscopy

The infrared spectra (Figure 4) show bands in the region between 1400 cm^{-1} – 400cm^{-1}, which is the crucial part for boron and sulfur centered oxygen tetrahedra and indicates their presence (full spectrum in Figure S7).[30] The respective bands are tentatively assigned on the basis of previous calculations on borosulfates (Table S7).[10,31] The asymmetric stretching vibrations ν_{asym}(S-O) range from 1388–1211 cm^{-1}. The symmetric stretching vibrations ν_{sym}(B–O) peak at 1103 and 1041 cm^{-1}, whereas the band at 1020 cm^{-1} is assigned to asymmetric vibrations ν_{asym}(B–O). The bands between 975–954 cm^{-1} are referred to asymmetric bending vibrations δ_{asym}(O–B–O) and the symmetric stretching vibration ν_{sym}(S–O) occurs at 817 cm^{-1}. The asymmetric bending vibration δ_{asym}(O–S–O) ranges from 746–669 cm^{-1}. Between 634–518 cm^{-1} asymmetric bending vibrations δ_{asym}(O–B–O), δ_{asym}(O–S–O) occur as well as bridging bending vibrations. The region below 500 cm^{-1} is mainly attributed to asymmetric bending vibrations δ_{asym}(O–S–O).

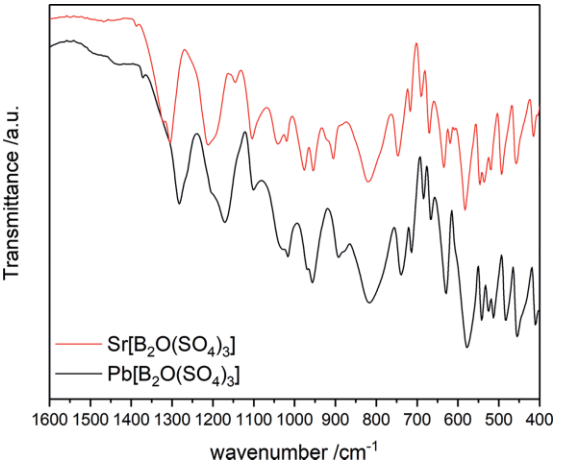

Figure 4. Infrared spectra of $Sr[B_2O(SO_4)_3]$ (red) and $Pb[B_2O(SO_4)_3]$ (black).

DFT Calculation

To understand the electronic structures of $M[B_2O(SO_4)_3]$ (*M* = Sr, Pb), a DFT calculation has been employed. The optimized crystal structures agree well with the experimentally refined cell parameters, indicating small differences of less than 1 % for both the $Sr[B_2O(SO_4)_3]$ and $Pb[B_2O(SO_4)_3]$ structures. Calculating the electronic structure of both compounds reveals that they are wide band gap insulators with the Fermi level falling at the top of band composed primarily of oxygen 2p orbitals, as shown in Figure 5. To ensure the accuracy of band gaps, a hybrid functional (HSE06) calculation was subsequently performed to determine a more precise E_g of 9.6 eV for $Sr[B_2O(SO_4)_3]$ and 5.6 eV for $Pb[B_2O(SO_4)_3]$. This is well in accordance with the experimentally determined band gap E_g =

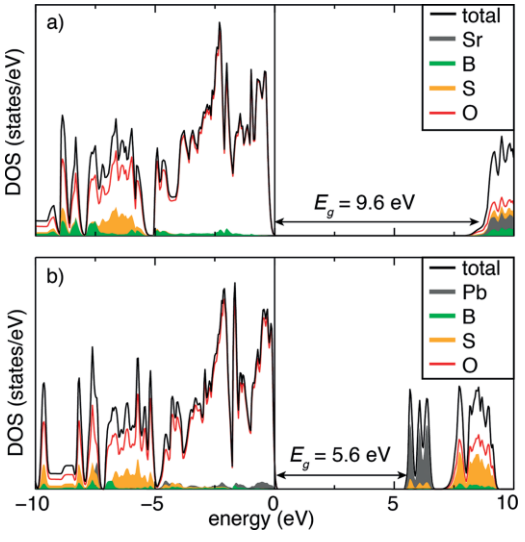

Figure 5. (a) Density of states of $Sr[B_2O(SO_4)_3]$. The total density of states is shown by the black line, while the partial DOS is shown gray, green, yellow and red for Sr, B, S, and O, respectively. (b) Total and partial DOS of $Pb[B_2O(SO_4)_3]$. The total density of states is shown in by the black line, while the partial DOS is shown gray, green, yellow, and red for Pb, B, S, and O, respectively.

5.4(1) eV of $Pb[B_2O(SO_4)_3]$ (Fig S8). As the band gap of $Sr[B_2O(SO_4)_3]$ lies in the VUV, we did not confirm the band gap experimentally.

Decomposing the total electronic density of states (DOS) into its component orbitals show the metal cations are mainly populated in conduction band, while B, S, and O are spread across the entire energy range examined.

Atomic interactions between atoms were visualized by calculating the electron localization function (ELF) for $M[B_2O(SO_4)_3]$ (Figure 6). High values of ELF around the B–O bond indicate the covalent nature of the interaction, as well as strong localization near Pb and O.

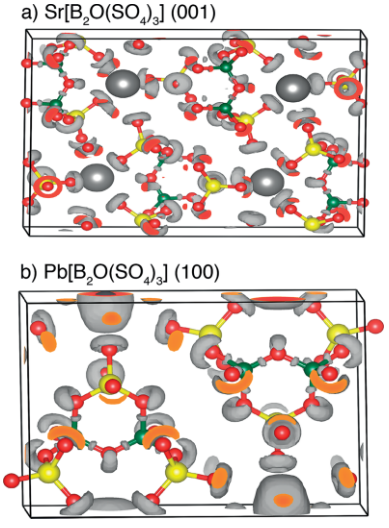

Figure 6. a) ELF of $Sr[B_2O(SO_4)_3]$ along the (001) plane. b) ELF of $Pb[B_2O(SO_4)_3]$ along the (100) plane. Metal cations, B, S and O atoms are shown in gray, green, yellow, and red, respectively.

The Born effective charge (Z*) was also calculated because it is an indicator of the possible stereochemical activity for a compound of lone pairs. The values for the main group metals in $M[B_2O(SO_4)_3]$ (M = Sr, Pb) are provided in Table 3. Comparing the calculated Born effective charge with formal valence illustrates the tendency for polarization of lone pairs on ions. For example, the Z* values, calculated by the Berry phase method, are in great agreement with nominal charge states of ions that are not polarized, such as halides. Here, the Z* values for Sr^{2+} and Pb^{2+} are larger than their formal valence charges. In the case of the lead cation, specifically, the fact that Z* is not significantly implies there is only a weak tendency of polarization by the Pb^{2+} lone pair.

Table 3. The Born effective charges of metals in $M[B_2O(SO_4)_3]$ (M = Sr, Pb).

Metals	Z^*_{xx}	Z^*_{yy}	Z^*_{zz}
Sr1	3.45	3.32	3.77
Sr2	3.45	3.32	3.76
Pb1	3.39	3.68	3.71
Pb2	3.39	3.68	3.71

The linear optical properties were calculated from the frequency dependent complex dielectric response (Figures 7 and 8).

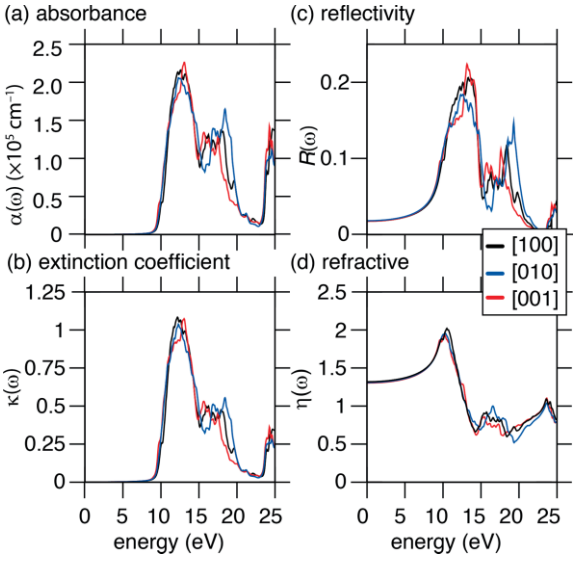

Figure 7. a) Absorbance, b) extinction coefficient, c) reflectivity, and d) refractive spectrum calculated based on the frequency-dependent complex dielectric function for $Sr[B_2O(SO_4)_3]$.

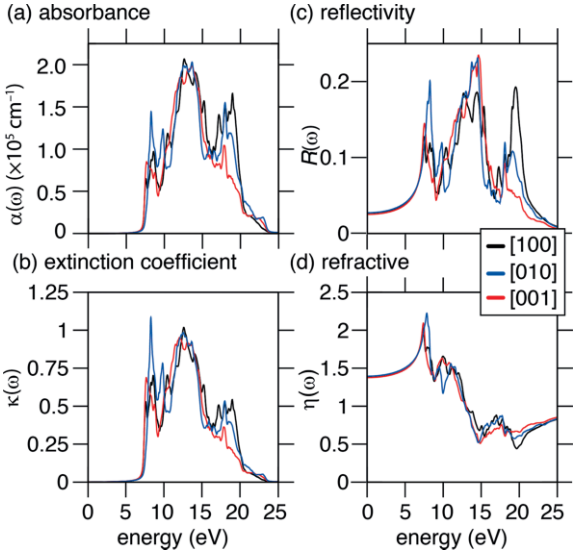

Figure 8. (a) Absorbance, (b) extinction coefficient, (c) reflectivity, and (d) refractive spectrum calculated based on the frequency-dependent complex dielectric function for $Pb[B_2O(SO_4)_3]$.

Thermogravimetric Analysis

The thermal stability of the title compounds was investigated by TGA (Figure 9). $Sr[B_2O(SO_4)_3]$ starts to decompose around 450 °C and the decomposition is completed at 630 °C with an observed mass loss of 37.4 %. This corresponds well to a formal loss of two molecules of SO_3 ($\Delta m_{calc.}$ = 38.7 %) leading to Equation (1):

$$Sr[B_2O(SO_4)_3] \rightarrow SrSO_4 + B_2O_3 + 2\ SO_3 \quad (1)$$

However, the decomposition may be divided into two steps (shoulder in Figure 9) indicating an intermediate phase. We suggest the decomposition to a lower condensed borosulfate as

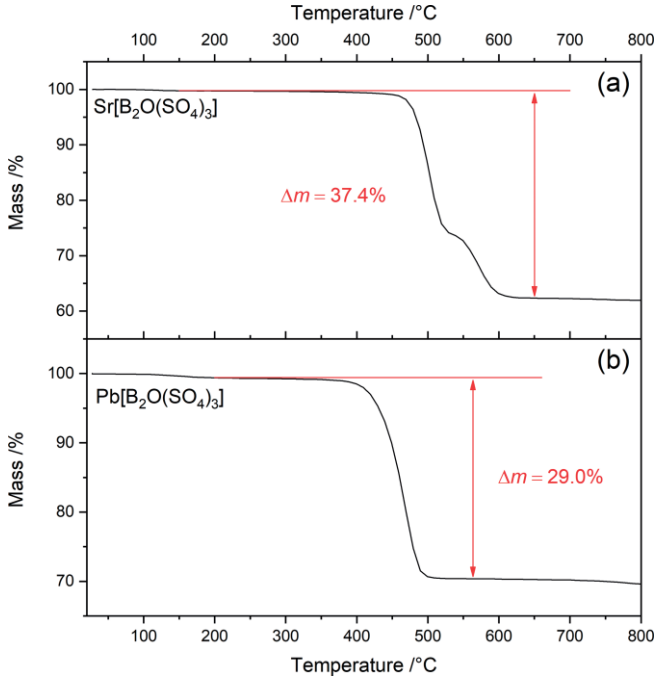

Figure 9. Thermogravimetric analysis of $Sr[B_2O(SO_4)_3]$ (a) and $Pb[B_2O(SO_4)_3]$ (b) under nitrogen atmosphere.

observed for $K_3[B(SO_4)_3]$ towards $K_5[B(SO_4)_4]$.[2] Thus, formation of the theoretical intermediate phase $Sr_5[B(SO_4)_4]_2$ would cause a mass loss of $\Delta m_{calc.}$ = 27.1 wt.-% ($\Delta m_{obs.}$ = 26.1 wt.-%) [Equation (2)].

$$5\ Sr[B_2O(SO_4)_3] \rightarrow Sr_5[B(SO_4)_4]_2 + 4\ B_2O_3 + 7\ SO_3 \quad (2)$$

$\Delta m_{calc.}$ = 27.1 wt.-%$\Delta m_{obs.}$ = 26.1 wt.-%

A consequent decomposition towards the sulfate would result in a further mass loss of $\Delta m_{calc.}$ = 11.7 wt.-% ($\Delta m_{obs.}$ = 11.3 wt.-%) [Equation (3)].

$$Sr_5[B(SO_4)_4]_2 \rightarrow 5\ SrSO_4 + B_2O_3 + 3\ SO_3 \quad (3)$$

$\Delta m_{calc.}$ = 11.7 wt.-%$\Delta m_{obs.}$ = 11.3 wt.-%

$Pb[B_2O(SO_4)_3]$ decomposes within one apparent step starting at around 400 °C, similar to Equation (1). The observed mass loss of 29.0 % is in accordance to the theoretical mass loss of $\Delta m_{calc.}$ = 30.0 %. Presumably the respective intermediate phase has a lower thermal stability and hence cannot be formed under these conditions. A similar decomposition behavior was reported for $Ba[B_2O(SO_4)_3]$ with a decomposition temperature of 480 °C.[11]

Conclusions

Herein, we reported the crystal structures of the very first strontium borosulfate $Sr[B_2O(SO_4)_3]$ and a novel lead borosulfate $Pb[B_2O(SO_4)_3]$. $Pb[B_2O(SO_4)_3]$ crystallizes in a new structure type and is closely related to $Sr[B_2O(SO_4)_3]$, which crystallizes isotypically with $Ba[B_2O(SO_4)_3]$.[11] Both structures consist of loop branched *zweier* double chains but differ in their orientation. Similarities can be found in the minerals *stillwellite* $CeBO[SiO_4]$ and *tremolite* $Mg_4Ca_2[Si_4O_{11}]_2(OH)_2$, which emphasizes the analogy to silicates.

The reason for the different orientation of the chains in $Sr[B_2O(SO_4)_3]$ and $Pb[B_2O(SO_4)_3]$ might be a lone pair activity, which becomes noticeable by the elongated two Pb–O distances towards the respective upper chain. However, the DFT calculations only showed a weak polarization of the lone pair, which is most probably due to the weak coordination behavior of the borosulfate anion. In the previously reported $Pb[B_2(SO_4)_4]$ no significant deviations between the different Pb–O bonds were found. Therein, the authors claimed, that the lone pair activity was suppressed by the rigidity of the rod-shaped chains. In contrast, the herein discussed $Pb[B_2O(SO_4)_3]$ shows a larger coordination environment {CN = 10 with respect to CN = 8 in $Pb[B_2(SO_4)_4]$} and the presence of less symmetrically shaped chains might enable a slight polarizability, due to a different orientation of the chains.

Thermal analysis of $Sr[B_2O(SO_4)_3]$ and $Pb[B_2O(SO_4)_3]$ revealed decomposition temperatures of $T_{decomp.}$ 450 °C and $T_{decomp.}$ 400 °C, respectively. According to our previous postulation for the thermal stabilities of borosulfates, this is in the expected range for chain like borosulfates with divalent metal cations.

Further investigations will focus on the doping of divalent Eu^{2+} in $Sr[B_2O(SO_4)_3]$, comprising a proper host and is expected to show weak ligand field splitting and a weak nephelauxetic effect, based on our previous findings on optical properties of borosulfates.

Experimental Section

Synthetic Procedure: $M[B_2O(SO_4)_3]$ (M = Sr, Pb) was synthesized on the basis of refs..[3,11] 3 mmol $B(OH)_3$ were dissolved in 2.5 mL of H_2SO_4 in a Schlenk flask under nitrogen flow at 200 °C for 1 h. After cooling down to 120 °C, 0.3 mL of Oleum (65 %) was added. Subsequently, 1 mmol of the respective anhydrous metal chloride was added and after the vigorous reaction is completed, the solution was transferred into a silica glass ampule (outer diameter: 1.2 cm, wall thickness: 0.1 cm) and fused. The ampule was placed in a muffle furnace applying the following temperature program: heating to 300 °C with 100 °C/h, holding the temperature for 96 h and cooling down to room temperature with 50 °C/h.

Several single-crystals were formed above the acid as well as a polycrystalline bulk in the acid (Figure S6). Ampoules were opened after freezing with liquid nitrogen. The bulk excess of the acid was pipetted, whereas the adhesive acid was evaporated at 300 °C. The crystals are very sensitive to moisture and were accordingly stored under inert conditions. Phase purity was confirmed by powder XRD (Figure 10).

Crystal Structure Determination: Immediately after opening the ampoule, single-crystals were transferred into perfluorinated polyether and selected for single-crystal XRD. Diffraction data for all compounds were collected with a Bruker D8 Venture diffractometer using Mo-K_α radiation (λ = 0.71073 Å). The temperature was adjusted with a nitrogen flow (Oxford Cryosystems). The absorption correction was performed employing the multi-scan method; then the crystal structures were solved with direct methods and refined by the full-matrix least-squares technique within the SHELXTL program.[32] $Sr[B_2O(SO_4)_3]$ was refined as a non-merohedral twin with a ratio 0.30(11):70(11) (twin matrix 0 0 –1 0 –1 0 –1 0 0). Crystal data and details of the structure refinements are listed in Table 4 as well as Tables S1–S4 in the Supporting Information.

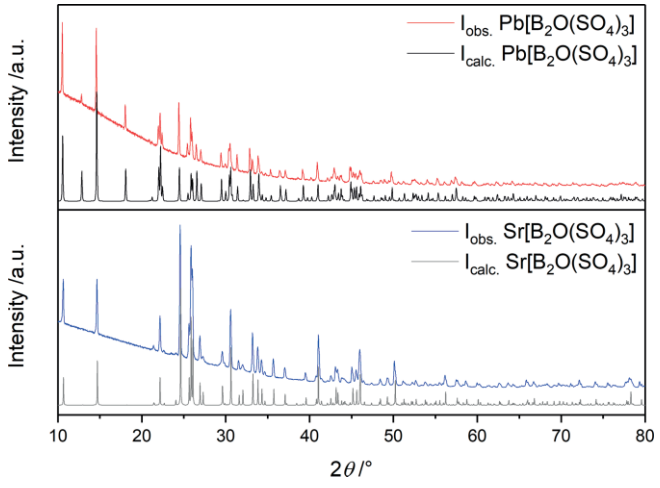

Figure 10. Observed PXRD pattern in comparison to the calculated ones for $Pb[B_2O(SO_4)_3]$ (top) and $Sr[B_2O(SO_4)_3]$ (bottom).

Table 4. Crystal data and details of the structure refinements (esds in parentheses).

	$Sr[B_2O(SO_4)_3]$	$Pb[B_2O(SO_4)_3]$
Temperature/K	200(2)	201(2)
Molar weight/g mol^{-1}	413.45	532.99
Crystal system	orthorhombic	monoclinic
Space group	*Pnma* (No. 62)	$P2_1/m$ (No. 11)
Crystal shape	block	block
Crystal size/mm^3	0.056x0.108x0.300	0.053x0.082x0.114
Color	colorless	colorless
a/pm	1657.38(27)	440.00(2)
b/pm	1203.68(19)	1210.19(5)
c/pm	439.484(8)	860.43
β/°		103.587
Volume/10^6 pm^3	876.776(16)	445.34(3)
Z	4	2
Calculated density D_x/g cm^{-3}	3.132	3.975
Absorption coefficient μ/mm^{-1}	6.949	19.729
F(000)	800	488
Radiation (λ/Å)	0.71073	0.71073
Diffractometer	Bruker D8 Venture	Bruker D8 Venture
Absorption correction	multi-scan	multi-scan
Transmission factor (min./max.)	0.4990/0.7489	0.5891/0.7483
Index range *h*|*k*|*l* (min./max.)	–23/0|-16/0|-6/0	–8/8|-22/22|-16/16
Theta range/°	2.458 < Θ < 29.986	2.435 < Θ < 42.280
Reflections collected	1334	16743
Independent reflections	1334	3267
Observed reflections ($I > 2\sigma$)	1269	2973
R_{int}		0.0373
Refined parameters	89	94
R_1 (all data)	0.0414	0.0258
wR_2 (all data)	0.0982	0.0400
GooF	1.307	1.097
Residual electron density (min./max.) /e$^-$ Å^{-3}	–0.594/2.268	–2.325/1.291

Further details of the crystal structure investigation(s) may be obtained from Fachinformationszentrum Karlsruhe, 76344 Eggenstein-Leopoldshafen, Germany (fax: +49-7247-808-259; E-mail: crysdata@fiz-karlsruhe.de, http://www.fiz-karlsruhe.de/request_for_deposited_data.html), on quoting the deposition numbers CSD-1923046 {for $Sr[B_2O(SO_4)_3]$} and 1923047 {for $Pb[B_2O(SO_4)_3]$}.

X-ray Powder Diffraction: The samples were ground and filled into a Hilgenberg glass capillary (outer diameter 0.3 mm, wall thickness 0.01 mm) inside a glovebox. The data was collected with a Bruker D8 Advance diffractometer with Cu-K_α radiation (λ = 1.54184) with a 1D LynxEye detector.

Infrared Spectroscopy: The infrared spectra were recorded using a Bruker EQUINOX 55 FT-IR spectrometer equipped with a platinum ATR setup in a range of 4000–400 cm^{-1}.

Optical Spectroscopy: The optical reflection spectra were measured with a Varian Cary 300 Scan UV/Vis spectrophotometer in the range of 200–800 nm.

Thermal Analysis: The thermogravimetric analysis was done in alumina crucibles employing a NETZSCH STA 409 PC Luxx in nitrogen atmosphere and a heating ramp of 10 K/min.

DFT Calculations: Electronic structure calculations on $M[B_2O(SO_4)_3]$ (M = Sr, Pb) were performed using Density Functional Theory (DFT) within the Vienna ab initio Simulation Package (VASP).[33] The calculations employed a plane-wave basis set and projector-augment-wave (PAW) potentials.[34] The generalized gradient approximation (GGA) was used with exchange and correlation described by the Perdew–Burke–Ernzerhof (PBE) functional. The total energy calculations used a cutoff energy of 500 eV, a 4×4×4 Γ-centered Monkhorst–Pack k-point grid, and convergence criteria of 1×10^{-8} eV and 1×10^{-6} eV for the electronic and structure relaxation, respectively. The band gap of $M[B_2O(SO_4)_3]$ (M = Sr, Pb) was additionally evaluated with the Heyd-Scuseria–Ernzerhof screened hybrid exchange and correlation functional, HSE06, which implements a mixture of PBE (75 %) and Hartree–Fock exact exchange (25 %) and a range-separation of 0.2 Å.[35] Subsequently, the optical properties were calculated based on the frequency dependent dielectric response including local field effects in the random-phase approximation (RPA).[36] Electron localization function (ELF) was also carried out on the compounds for examining the charge distribution and bonding in the crystal structures.[37] ELF calculations were visualized using VESTA.[38]

Acknowledgments

The authors thank the Deutsche Forschungsgemeinschaft (DFG) for financial support under the project HO 4503/5-1. P. N. thanks the Fonds der Chemischen Industrie (FCI) for a Ph.D. fellowship.

Keywords: Borosulfates · Strontium · Lead · Silicate-analogous materials

[1] H. A. Höppe, K. Kazmierczak, M. Daub, K. Förg, F. Fuchs, H. Hillebrecht, *Angew. Chem. Int. Ed.* **2012**, *51*, 6255–6257; *Angew. Chem.* **2012**, *124*, 6359.
[2] M. Daub, K. Kazmierczak, P. Gross, H. Höppe, H. Hillebrecht, *Inorg. Chem.* **2013**, *52*, 6011–6020.
[3] P. Netzsch, P. Gross, H. Takahashi, H. A. Höppe, *Inorg. Chem.* **2018**, *57*, 8530–8539.
[4] P. Netzsch, M. Hämmer, P. Gross, H. Bariss, T. Block, L. Heletta, R. Pöttgen, J. Bruns, H. Huppertz, H. A. Höppe, *Dalton Trans.* **2019**, *110*, 3250.
[5] a) H. A. Höppe, *Angew. Chem. Int. Ed.* **2009**, *48*, 3572–3582; *Angew. Chem.* **2009**, *121*, 3626–3636; b) T. Jüstel, H. Nikol, C. Ronda, *Angew. Chem.* **1998**, *110*, 3250–3271; c) Y.-C. Lin, M. Karlsson, M. Bettinelli, *Top. Curr. Chem.* **2016**, *374*, 21; d) M. Sato, S. W. Kim, Y. Shimomura, T. Hasegawa, K. Toda, G. Adachi, *Handbook on the physics and chemistry of rare earths* **2016**, *49*, 1–128.
[6] a) H. A. Höppe, H. Lutz, P. Morys, W. Schnick, A. Seilmeier, *J. Phys. Chem. Solids* **2000**, *61*, 2001–2006; b) R. Mueller-Mach, G. Mueller, M. R. Krames,

H. A. Höppe, F. Stadler, W. Schnick, T. Jüstel, P. Schmidt, *Phys. Status Solidi A* **2005**, *202*, 1727–1732.
[7] V. Bachmann, T. Jüstel, A. Meijerink, C. Ronda, P. J. Schmidt, *J. Lumin.* **2006**, *121*, 441–449.
[8] M. Zhang, J. Wang, W. Ding, Q. Zhang, Q. Su, *Appl. Phys. B* **2007**, *86*, 647–651.
[9] R. D. Shannon, *Acta Crystallogr., Sect. A* **1976**, *32*, 751–767.
[10] J. Bruns, M. Podewitz, M. Schauperl, B. Joachim, K. R. Liedl, H. Huppertz, *Chem. Eur. J.* **2017**, *23*, 16773–16781.
[11] P. Gross, A. Kirchhain, H. A. Höppe, *Angew. Chem. Int. Ed.* **2016**, *55*, 4353–4355; *Angew. Chem.* **2016**, *128*, 4426.
[12] G. Schott, H. U. Kibbel, *Z. Anorg. Allg. Chem.* **1962**, *314*, 104–112.
[13] S. Schönegger, J. Bruns, B. Gartner, K. Wurst, H. Huppertz, *Z. Anorg. Allg. Chem.* **2018**, *644*, 1702–1706.
[14] a) R. Kniep, G. Gözel, B. Eisenmann, C. Röhr, M. Asbrand, M. Kizilyalli, *Angew. Chem. Int. Ed. Engl.* **1994**, *33*, 749–751; *Angew. Chem.* **1994**, *106*, 791; b) Y. Shi, J. Liang, H. Zhang, Q. Liu, X. Chen, J. Yang, W. Zhuang, G. Rao, *J. Solid State Chem.* **1998**, *135*, 43–51; c) A. B. Ali, E. Antic-Fidancev, B. Viana, P. Aschehoug, M. Taibi, J. Aride, A. Boukhari, *J. Phys. Condens. Matter* **2001**, *13*, 9663–9671.
[15] T. Schlieper, W. Milius, W. Schnick, *Z. Anorg. Allg. Chem.* **1995**, *621*, 1380–1384.
[16] P. Bielec, R. Nelson, R. P. Stoffel, L. Eisenburger, D. Günther, A.-K. Henss, J. P. Wright, O. Oeckler, R. Dronskowski, W. Schnick, *Angew. Chem. Int. Ed.* **2019**, *58*, 1432–1436; *Angew. Chem.* **2019**, *131*, 1446–1450.
[17] a) S. G. Jantz, M. Dialer, L. Bayarjargal, B. Winkler, L. van Wüllen, F. Pielnhofer, J. Brgoch, R. Weihrich, H. A. Höppe, *Adv. Opt. Mater.* **2018**, *6*, 1800497; b) M. Luo, F. Liang, Y. Song, D. Zhao, N. Ye, Z. Lin, *J. Am. Chem. Soc.* **2018**, *140*, 6814–6817.
[18] W. Loewenstein, *Am. Mineral.* **1954**, *39*, 92–96.
[19] A. A. Voronkov, Y. A. Pyatenko, *Sov. Phys. Cryst.* **1967**, *12*, 214–220.
[20] G.-Y. Yang, S. C. Sevov, *Inorg. Chem.* **2001**, *40*, 2214–2215.
[21] F. C. Hawthorne, H. D. Grundy, *Can. Mineral.* **1976**, *14*, 334–345.
[22] T. Balić Žunić, E. Makovicky, *Acta Crystallogr., Sect. B* **1996**, *52*, 78–81.
[23] E. Makovicky, T. Balić-Žunić, *Acta Crystallogr., Sect. B* **1998**, *54*, 766–773.
[24] M. Daub, K. Kazmierczak, H. A. Höppe, H. Hillebrecht, *Chem. Eur. J.* **2013**, *19*, 16954–16962.
[25] M. Daub, H. Hillebrecht, *Eur. J. Inorg. Chem.* **2015**, 4176–4181.
[26] a) R. Hoppe, *Angew. Chem. Int. Ed.* **1966**, *5*, 95–106; *Angew. Chem.* **1966**, *78*, 52–63; b) R. Hoppe, *Angew. Chem. Int. Ed. Engl.* **1970**, *9*, 25–34; *Angew. Chem.* **1970**, *82*, 7; c) R. Hübenthal, *MAPLE*: Program for the Calculation of the Madelung Part of Lattice Energy; Universität Gießen, **1993**.
[27] D. Garske, D. R. Peacor, *Z. Kristallogr.* **1965**, *121*, 204–210.
[28] C. Logemann, M. S. Wickleder, *Angew. Chem. Int. Ed.* **2013**, *52*, 14229–14232; *Angew. Chem.* **2013**, *125*, 14479.
[29] S. M. Antao, *American Mineralogist* **2012**, *97*, 661–665.
[30] K. Nakamoto, *Infrared and Raman spectra of inorganic and coordination compounds*: Part A: Theory and applications in inorganic chemistry; Wiley, Hoboken, N.J, **2009**.
[31] J. Bruns, M. Podewitz, M. Schauperl, K. R. Liedl, O. Janka, R. Pöttgen, H. Huppertz, *Eur. J. Inorg. Chem.* **2017**, 3981–3989.
[32] G. M. Sheldrick, *Acta Crystallogr., Sect. A* **2008**, *64*, 112–122.
[33] a) G. Kresse, J. Furthmüller, *Phys. Rev. B* **1996**, *54*, 11169–11186; b) G. Kresse, D. Joubert, *Phys. Rev. B* **1999**, *59*, 1758–1775.
[34] P. E. Blöchl, *Phys. Rev. B* **1994**, *50*, 17953–17979.
[35] J. Heyd, G. E. Scuseria, M. Ernzerhof, *J. Chem. Phys.* **2003**, *118*, 8207–8215.
[36] J. Harl, G. Kresse, *Phys. Rev. Lett.* **2009**, *103*, 56401.
[37] a) A. Savin, R. Nesper, S. Wengert, T. F. Fässler, *Angew. Chem. Int. Ed. Engl.* **1997**, *36*, 1808–1832; *Angew. Chem.* **1997**, *109*, 1892; b) M. Kohout, F. R. Wagner, Y. Grin, *Theo. Chem. Acc.* **2002**, *108*, 150–156.
[38] K. Momma, F. Izumi, *J. Appl. Crystallogr.* **2011**, *44*, 1272–1276.

Received: July 31, 2019